ELSEVIER

International Journal of Solids and Structures 41 (2004) 5871–5884

INTERNATIONAL JOURNAL OF SOLIDS and STRUCTURES

www.elsevier.com/locate/ijsolstr

Macro- and micro-behaviors of granular materials under different sample preparation methods and stress paths

Tang-Tat Ng *

Civil Engineering Department, University of New Mexico, Albuquerque, NM 87131, USA

Received 6 May 2004

Abstract

A series of numerical drained tests have been performed to study the macroscopic and microscopic behaviors of granular materials prepared by three different techniques (isotropic compression, tamping, and dry pluviation). The samples consist of two kinds of ellipsoids with 1170 particles. The two kinds are equal by weight. The aspect ratios (major axis length/minor axis length) of these two kinds are 1.2 and 1.5, respectively. All samples were subjected to an isotropic confining pressure of 100 kPa before loaded along 11 different stress paths. The shear strengths of these drained tests were compared with two published yield models. Good agreement was found in general. One model showed an error of less than 5% for 90% of the time. Two microscopic parameters, the unit contact normal and the contact normal force, were examined for all specimens during axial compression loading. The principal stress ratio was found to correlate better with the contact normal force than the unit contact normal. The evolution of this microscopic descriptor was further investigated for all drained tests. The result showed a unique relationship between the strength descriptor of the contact normal force and the principal stress ratio. Excellent correlations were found for the drained tests with various intermediate stresses.

Keywords: Granular media; Micro-mechanics; Numerical methods

1. Introduction

Soil samples behave differently when they are prepared using different sample preparation procedures. It is well known that different behaviors arise from samples with similar void ratios but different fabrics. However, obtaining soil fabrics by physical measurements is extremely difficult. In addition, examining the fabric evolution of a sample by any destructive methods required multiple samples which may introduce data scattering. Multi-samples are inevitable when studying the effect of stress path. These difficulties can be avoided easily by using the numerical method. The discrete element method (DEM), a numerical method, has demonstrated the ability to study granular materials. DEM has been used to examine the fabric of

* Tel.: +1-505-277-4844; fax: +1-505-277-1988.
E-mail address: tang@unm.edu (T.-T. Ng).

0020-7683/$ - see front matter © 2004 Elsevier Ltd. All rights reserved.
doi:10.1016/j.ijsolstr.2004.05.050

granular samples generated with identical preparation process (Rothenburg and Bathurst, 1992; Ng, 1999, 2001). In this paper, we will use the DEM and the newly developed hydrostatic boundary to perform drained tests on samples of ellipsoids of two sizes that were prepared differently. The samples will display isotropic or anisotropic behavior based on their initial fabric. Drained tests along various stress paths were employed to study the effect of stress path. The macroscopic results were compared with two existing failure models. The microscopic results of these samples will also be examined.

2. Numerical program

Program ELLIPSE3H was employed to conduct numerical triaxial drained tests. At the contact between particles, the conventional non-linear, force dependent contact laws (Herzian normal law and simplified Mindlin's tangential law) were used (Lin and Ng, 1997). The contact between the particle and the boundary was calculated based on the recently developed hydrostatic boundary mechanism (Ng, 2002). Gravitational constants were set to zero with the exception of one particular sample during preparation phase. The properties of the ellipsoids are $G = 29$ GPa, $v = 0.15$, and $\mu = 0.5$.

2.1. Numerical samples

Three samples were created. They are made of two different types of ellipsoids. The minor axis lengths of these two types (I and II) are identical. The major axis length of Type II is larger than that of Type I. Type I is a smaller particle with an aspect ratio (AR) of 1.2. Type II particles have an AR of 1.5. The weights of all Type I and all Type II particles are the same in each sample. The total number of particles is 1170. A previous study has shown that the behavior is very similar for specimens with 999–9999 particles (Ng, 2004).

2.1.1. Sample preparation

The sample preparation contains two phases: particle generation and compression (densification). In the particle generation phase, larger Type II particles were randomly generated first. Type I (smaller) particles were then generated between the existing large particles. The particles of Sample A were randomly generated inside a cubic box. Then, the sample is isotropically compressed with a confining pressure of 100 kPa. The particles of Sample B were randomly generated inside a rectangular prism. Then, gravity was introduced to densify the sample (similar to the dry pluviation method). Finally, the gravity field was removed and the sample was consolidated with a confining pressure of 100 kPa. Sample C was created by vertically compressing the initial generated configuration of Sample B (similar to tamping method with only one layer). Then, the sample was isotropically consolidated to 100 kPa. The final configurations of these three samples are shown in Fig. 1.

As shown in Fig. 1, no distinguish feature can be identified from the appearance of these three samples. Table 1 lists the void ratio and coordination number of each sample. The void ratios of these three samples are comparable. The coordination number is the ratio between the number of particle contacts and the number of particles. The wall–particle contacts are not considered in the coordination number. As shown in Table 1, the coordination number of the gravity deposited Sample B is much lower than the other two samples that were densified by a boundary movement or gravity.

2.2. Testing method

A series of 11 drained tests were conducted on each sample. There are 33 strain-controlled tests entirely. The drained tests are divided into two groups for presentation. The qualitative changes in principal stresses

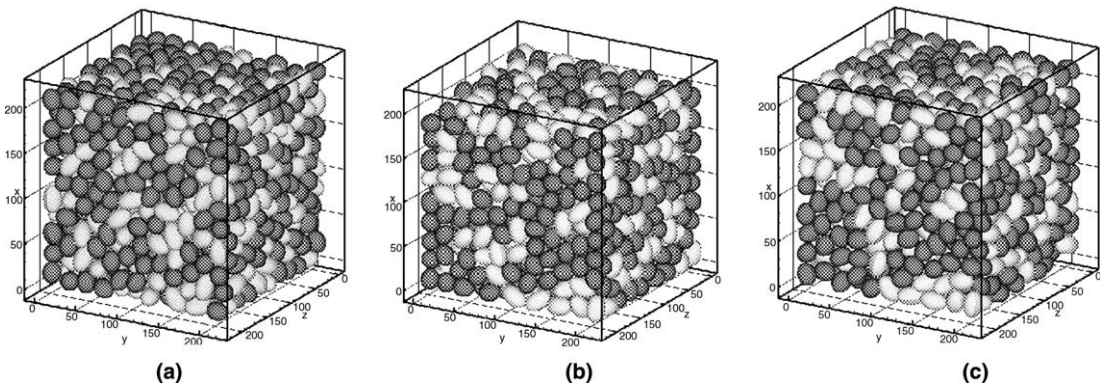

Fig. 1. Configurations of (a) Sample A, (b) Sample B, and (c) Sample C.

Table 1
Characteristics of three samples

Sample	Void ratio	Coordination number
A	0.639	5.913
B	0.634	4.556
C	0.631	5.802

Table 2
Changes of principal stresses in drained tests along various stress paths

	Drained tests						
	AE	CD	LC	LE	MSC	PS	TE
σ_v	$-\Delta\sigma$	$+\Delta\sigma$	Constant	Constant	$+\Delta\sigma$	$+\Delta\sigma$	$+\Delta\sigma$
σ_h^a	Constant	Constant	$+\Delta\sigma$	$-\Delta\sigma$	$-\Delta\sigma/2$	$+\Delta\sigma_2$[a]	$+\Delta\sigma$
σ_h^b	Constant	Constant	$+\Delta\sigma$	$-\Delta\sigma$	$-\Delta\sigma/2$	Constant	Constant

[a] $\Delta\sigma_2$ varies because $\varepsilon_2 = 0$.

of Group I are depicted in Table 2 (AE: axial extension test, CD: axial compression test, LC: lateral compression test, LE: lateral extension test, CMS: constant mean stress test, PS: plane strain test, and TE: triaxial extension test). Except the PS and TE tests, the other five tests (AE, CD, LC, LE, and CMS) can be

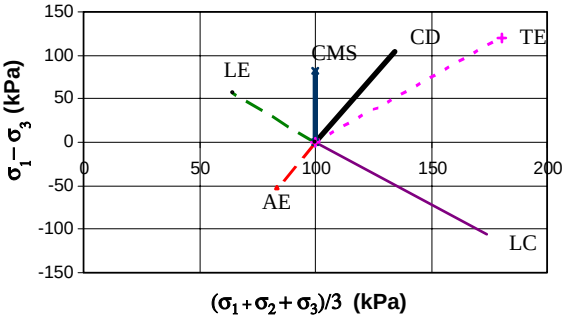

Fig. 2. Stress paths of six drained tests.

performed using conventional triaxial apparatus. The stress paths of these drained tests are shown in Fig. 2. Group II consists of constant-b drained tests, which are commonly used to investigate the effect of intermediate principal stress. They were performed by increasing the major principal stress (vertical stress) and controlling the intermediate and minor principal stresses such that $b = \frac{\sigma_2 - \sigma_3}{\sigma_1 - \sigma_3}$ is kept constant ($b = 0$, 0.2, 0.4, 0.6, 0.8, and 1) and $\sigma_3 = 100$ kPa. When $b = 0$ and $b = 1$, they are equivalent to the CD test ($\sigma_2 = \sigma_3$), and the TE test ($\sigma_2 = \sigma_1$), respectively. The stress path of a constant-b test is a linear line falls between the lines CD and TE in Fig. 2.

3. Macroscopic study

3.1. Friction angles of drained tests

The friction angles of these drained tests are presented in Fig. 3. The friction angle is defined as $\phi = \sin^{-1}(\frac{\sigma_1 - \sigma_3}{\sigma_1 + \sigma_3})$. Fig. 3a shows the result of Group I. In general, the order of the tests is PS, LC, TE, AE, LE, CD, and CMS when ranked by the friction angle. This is true for all three samples except the AE and LC tests of Sample C. It can be said that the sample preparation method does not significantly affect the relative difference in shear strength along various stress paths.

Fig. 3b shows the results of Group II. They are very similar to the laboratory observation of true triaxial tests. The shear strength increases with b to a maximum, beyond that the shear strength decreases. Similar trends are found in three samples. Thus, similar to the result of Group I, the effect of sample preparation from Group II is not significant on the overall shape of the curve for ϕ versus b.

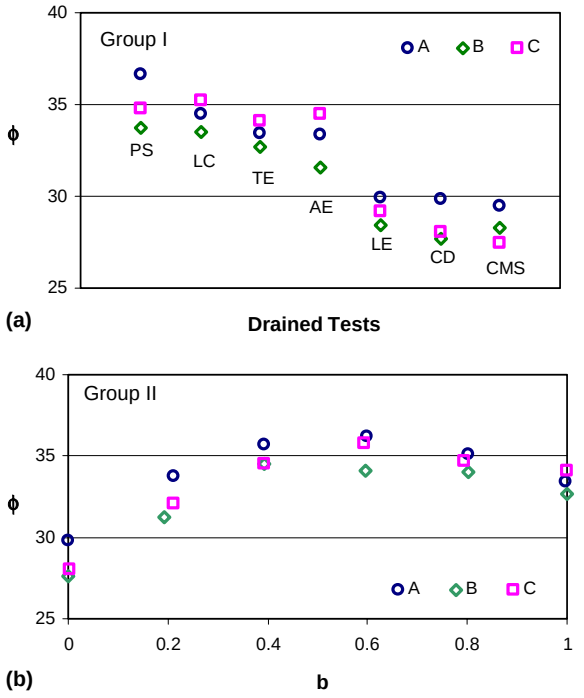

Fig. 3. Friction angles of drained tests of three samples.

The maximum differences in friction angles among these drained tests are 7.2°, 6.8°, and 8.3° for Samples A, B, and C, respectively. They are similar to the values observed in sands. The ratio of friction angles between compression and extension tests for these three samples ranges from 1.12 to 1.25. They are just slightly higher than the average value (1.12) of sands reported by Kulhaway and Mayne (1990). The present study demonstrated that the DEM simulations are very realistic.

To illustrate the degree of anisotropy the stress–strain curves of LC and TE tests of these samples were shown in Fig. 4. Sample A is an isotropic sample as the behaviors of LC and TE tests are very similar. The degree of anisotropy of Sample B is higher than that of Sample C. Samples prepared by gravity produce the highest degree of anisotropy.

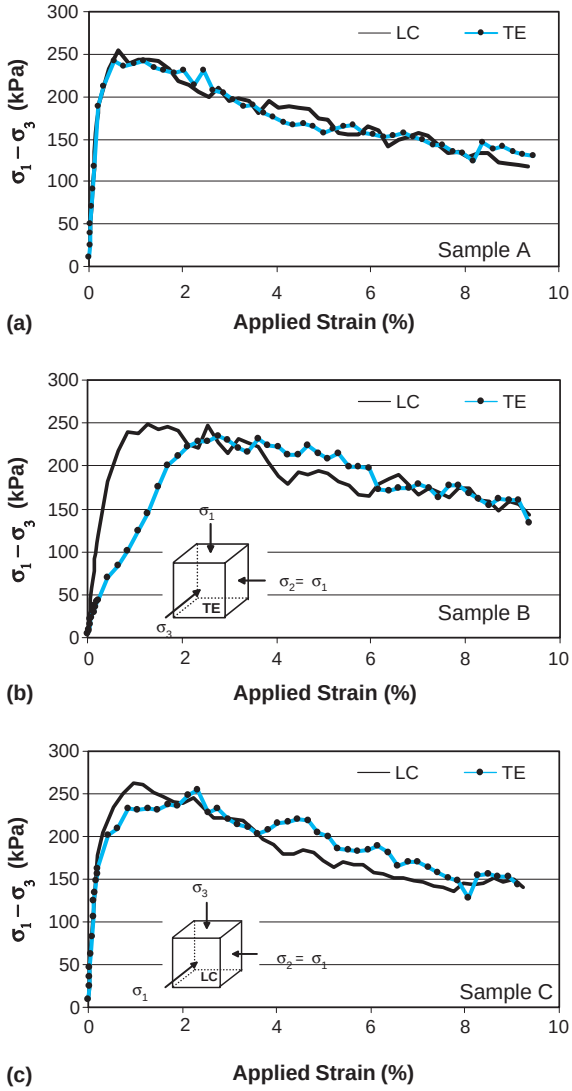

Fig. 4. The stress–strain curves of LC and TE for three specimens.

3.2. Comparison of failure criteria

Two failure criteria were used to compare with the DEM result. They were proposed by Lade (1977, 1984) and Ogawa and his colleagues (1974). Both models have two experimental constants. These two models have demonstrated good performance for isotropic samples (Ng, 2004). In this paper, we will examine the performance of these models for anisotropic samples. The two failure models in terms of the principal stresses (σ_1, σ_2, and σ_3) are:

(I) Lade model:

$$\left(\frac{(\sigma_1+\sigma_2+\sigma_3)^3}{\sigma_1\sigma_2\sigma_3}-27\right)\left(\frac{\sigma_1+\sigma_2+\sigma_3}{P_{\text{atm}}}\right)^m=\eta_1$$

where P_{atm} is the atmospheric pressure, m and η_1 are parameters that were determined from triaxial compression tests.

(II) Ogawa model:

$$\left(\frac{\sigma_1\sigma_2+\sigma_1\sigma_3+\sigma_2\sigma_3}{(\sigma_1+\sigma_2+\sigma_3)^2}\right)+n\left(\frac{3\sigma_1\sigma_2\sigma_3-(\sigma_1\sigma_2+\sigma_1\sigma_3+\sigma_2\sigma_3)(\sigma_1+\sigma_2+\sigma_3)}{3(\sigma_1+\sigma_2+\sigma_3)^3}\right)=\eta_2$$

where n and η_2 are constants.

The parameters of these two models were fitted by using three data points of the constant-b tests ($b = 0$, 0.2, and 0.4). The values of these parameters are shown in Table 3. The obtained formulas were then used to predict the shear strengths of the other three constant-b tests. Fig. 5 shows the comparison between the models and the DEM result of Group II. The circles are the numerical result. Excellent agreement as expected was found in Sample A, the maximum relative error ($\frac{\phi_{\text{predicted}}-\phi_{\text{measured}}}{\phi_{\text{measured}}}$) is only 2%. For Samples B and C, the models slightly degraded. The Ogawa model over predicted the friction angles for the anisotropic sample B. For the rest, both models under predict the friction angles in general. Nonetheless, the models still produced very good result for anisotropic samples since the relative error is less than 6%.

These models were also used to estimate the friction angles of the drained tests in Group I. Fig. 6 shows the overall performance of these two failure models. The heavy solid line is for zero relative error. The imaginary lines are for ±5% relative difference in friction angle. The two outside solid lines are for ±10% relative difference. Overall, the two models gave very satisfactory prediction. The prediction for the isotropic sample is shown as shaded squares. It indicates an excellent agreement. For anisotropic samples, the maximum error is about 12% in the LC and AE tests. Comparing Fig. 6a and b, the failure model proposed by Ogawa and his coworkers is slightly better. The prediction is within 5% of the actual values with the exception of three tests (the LC test on Sample B, and the LC and AE tests on Sample C).

Table 3
Parameters of the failure criteria

Sample	Failure models	
	Lade	Ogawa
A	$m = 0.061$, $\eta_1 = 15.804$	$n = -3.095$, $\eta_2 = 0.0663$
B[a]	$m = 0.000$, $\eta_1 = 12.168$	$n = -2.020$, $\eta_2 = 0.1470$
C[a]	$m = 0.000$, $\eta_1 = 12.194$	$n = -2.430$, $\eta_2 = 0.1167$

[a] The best fitted m value is negative, set $m = 0$.

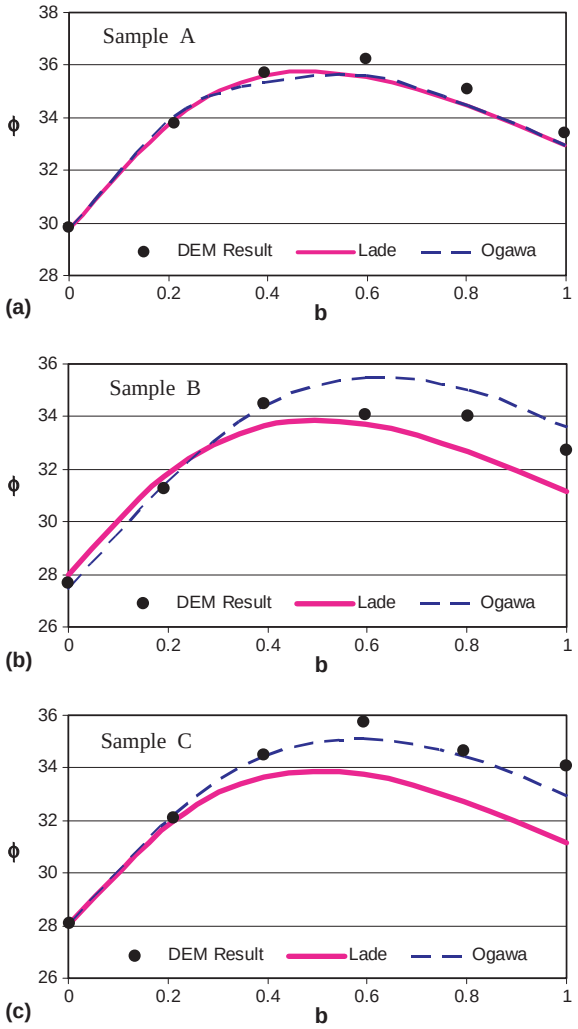

Fig. 5. Comparison between DEM simulations and the two failure models for Group II.

4. Micromechanical study

Fig. 7 shows the vector-typed microscopic parameters (particle orientation, branch vector, and contact normal) that are of interest. The particle orientation is the collection of the directions of the major axes of ellipsoids. The unit branch vector is the collection of unit vectors connecting the centers of two particles in contact. If the length is also considered, it is the branch length. Contact normal, N, is the collection of the unit contact normals. If the magnitude is also included, it is NF. They can be analyzed by the orientation tensor method. It will be described briefly in the following section. The orientation tensor method produces two fabric descriptors that are of great interest. A previous study (Ng, 2001) has revealed that one fabric descriptor (strength descriptor) of N is related well with the obliquity (σ_1/σ_3). In this paper, we will examine the strength descriptors of unit contact normal (N) and contact normal force (NF). Other microscopic parameters will be investigated in the future.

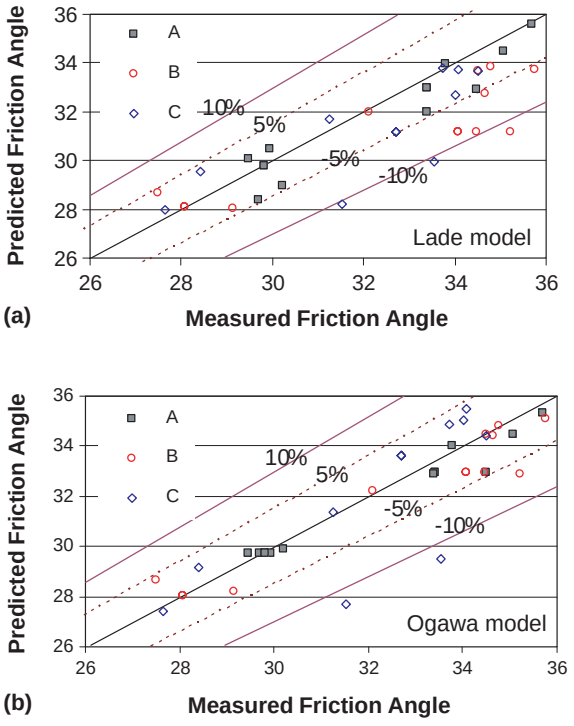

Fig. 6. Comparison of the two models and the DEM results.

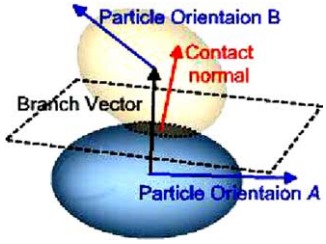

Fig. 7. Fabric parameters: particle orientation, branch vector, and contact normal.

4.1. Orientation tensor method

The components for the ith vector of N observations are (x_i, y_i, z_i). A 3×3 matrix of the sums of cross products of the components is

$$\frac{1}{N}\begin{bmatrix} \sum x_i^2 & \sum x_i y_i & \sum x_i z_i \\ \sum x_i y_i & \sum y_i^2 & \sum y_i z_i \\ \sum x_i z_i & \sum y_i z_i & \sum z_i^2 \end{bmatrix}$$

This matrix is called the orientation tensor when unit vectors are used (Scheidegger, 1965). Three eigenvalues (τ_1, τ_2, τ_3) and three eigenvectors can be computed from this matrix. The eigenvalues are a measure of

the degree of clustering data from the respective eigenvectors. These eigenvalues descriptively interpret the shape of the distribution of the data. Watson (1966) noted that clusters would tend to have $\tau_1 > \tau_2 \approx \tau_3$, and great-circle girdles $\tau_1 \approx \tau_2 > \tau_3$. Based on Woodcock's method, see Woodcock (1977), two descriptors (β_1 and β_2) can be used to identify and quantify the data. The two descriptors are defined as the strength descriptor ($\beta_1 = \ln\frac{\tau_1}{\tau_3}$) and the shape descriptor ($\beta_2 = \ln\frac{\tau_1}{\tau_2} / \ln\frac{\tau_2}{\tau_3}$). In this paper, the subscript 1 designates the strength descriptor that specifies the degree of preferred orientation and the subscript 2 (shape descriptor) indicates the shape between uniaxial clusters and uniaxial girdles.

4.2. Micromechanical result

There is a wealth of micro-information from these 33 drained tests which cannot be completely covered in this paper. Therefore, we will emphasize on two fabric descriptors N_1, and NF_1. The linkage between obliquity and these two fabric descriptors will be presented.

Figs. 8 and 9 illustrate the evolutions of the fabric descriptors of N and NF of these three samples subjected to axial compression loading. The behaviors of the strength descriptor (N_1 or NF_1) are similar in shape. It increases monotonically to a peak and is stationary. The initial drop of N_1 for Sample B is related to the principal direction change of the eigenvector. However, the behavior of shape descriptor (N_2, or NF_2) is very complex. Due to the wide range of NF_2, the NF_2 for Sample A was plotted on the second y-axis as shown in Fig. 9b. There are peaks but they are not related to the peak stress or the change from contraction to dilation in the volume change behavior. There is no change in shape since the values of N_2 (or NF_2) are larger than 1 always (Woodcock, 1977). The ups and downs are due to the variation of $\ln(\tau_1/\tau_2)$. The value of $\ln(\tau_2/\tau_3)$ increased monotonically with strain.

The effect of the magnitude of contact normal is illustrated in Fig. 10. The behavior of NF_1 is quite different from N_1 in magnitude although the overall shape is similar. The shape descriptors N_2 and NF_2 are

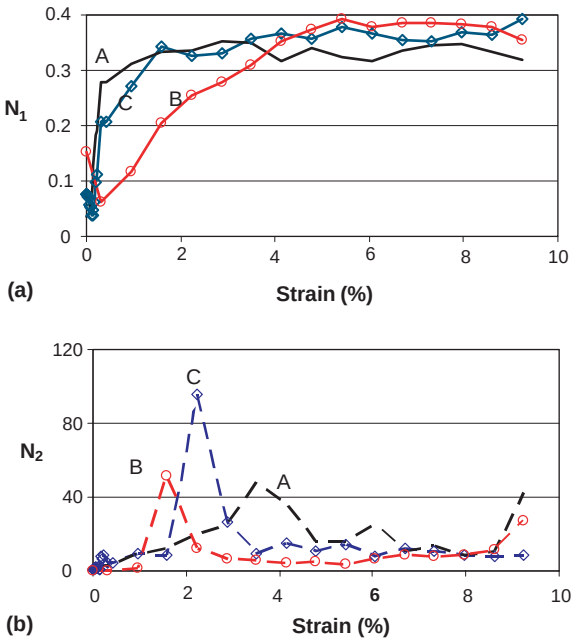

Fig. 8. Evolutions of fabric descriptors of unit contact normal.

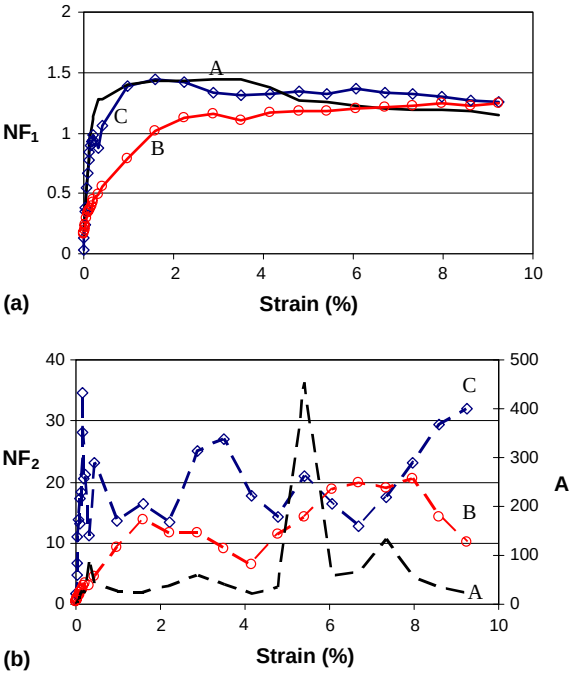

Fig. 9. Evolutions of fabric descriptors of NF.

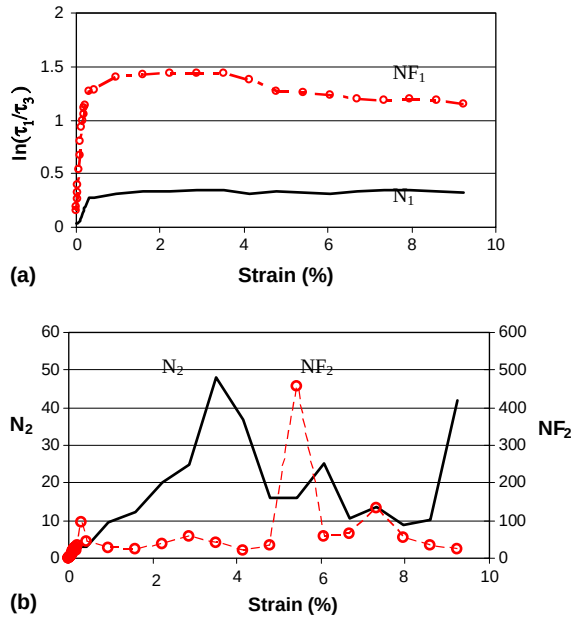

Fig. 10. Effect of the magnitude in contact normal for Sample A.

different in both magnitude and shape. To further discern the effect of the magnitude, the correlations between obliquity and N_1 (or NF_1) are plotted in Fig. 11 for all samples. The goodness of the fit to NF_1 is represented by the R^2 values that are also shown in the figure. The correlation is slightly better and for the isotropic sample A than the other anisotropic samples. Overall, a much simple relationship between the obliquity and NF_1 is evident. Therefore, NF_1 is a good candidate in the micromechanically based constitutive models.

The correlations between obliquity and NF_1 for Groups I and II are presented in Figs. 12 and 13, respectively. The data is less scattering for Group II (constant-b tests) than Group I. The solid curves are the best-fit curves to the data points. In sample A, the best fitting curve is linear. In Samples B and C, the best-fit curves are exponential. All the R^2 values are above 0.91. It can be said that the stress path does not affect the relationship between obliquity and NF_1.

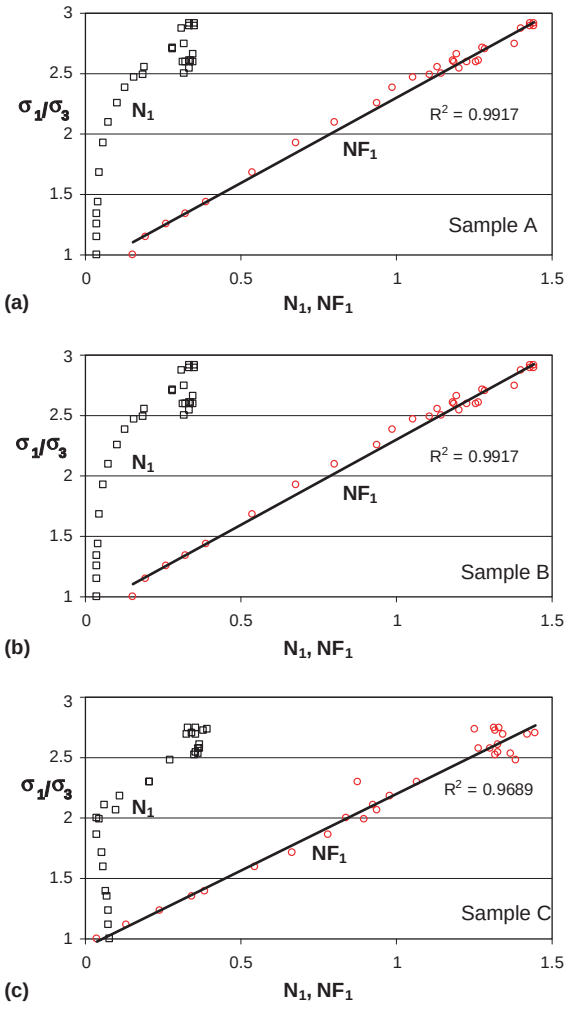

Fig. 11. Contact normal strength descriptor and obliquity for CD tests.

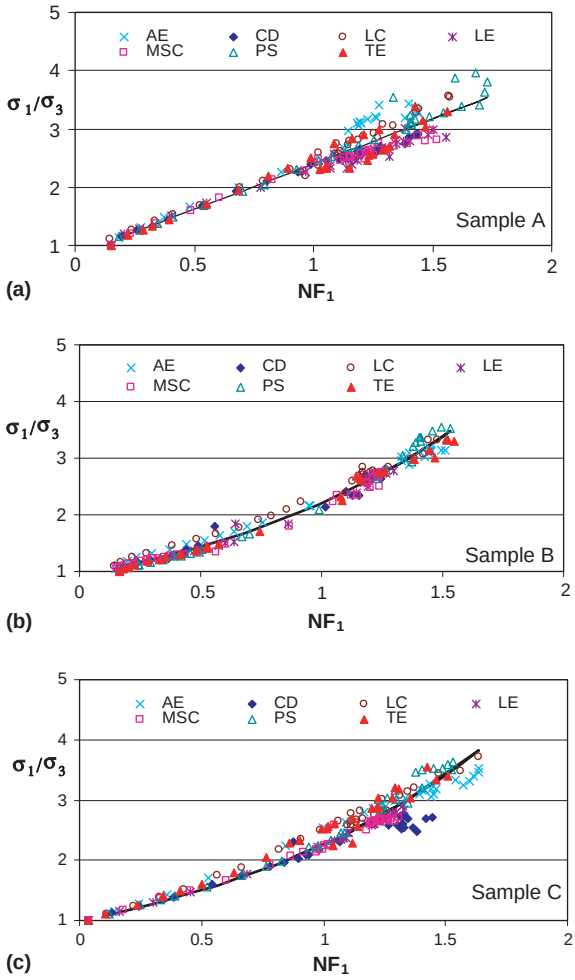

Fig. 12. Principal stress ratio versus NF_1 for Group I.

Overall, the above observation demonstrated that there is a unique linkage between the macroscopic parameter (obliquity) and the microscopic parameter (NF_1) is independent of the anisotropy of the sample and the loading path of the test.

5. Conclusions

Numerical drained tests were employed to study the effects of stress path and the intermediate principal stress on samples with different degrees of anisotropy. Three samples were prepared by three different sample preparation methods. The simulated behavior was similar to the laboratory observation in triaxial tests. They all demonstrated that the DEM with hydrostatic boundary simulates the triaxial tests accurately.

In the series of constant-b tests, the shear strength increased with b to a maximum, beyond that the shear strength decreased. This phenomenon has been observed in sands. The influence of anisotropy was found to

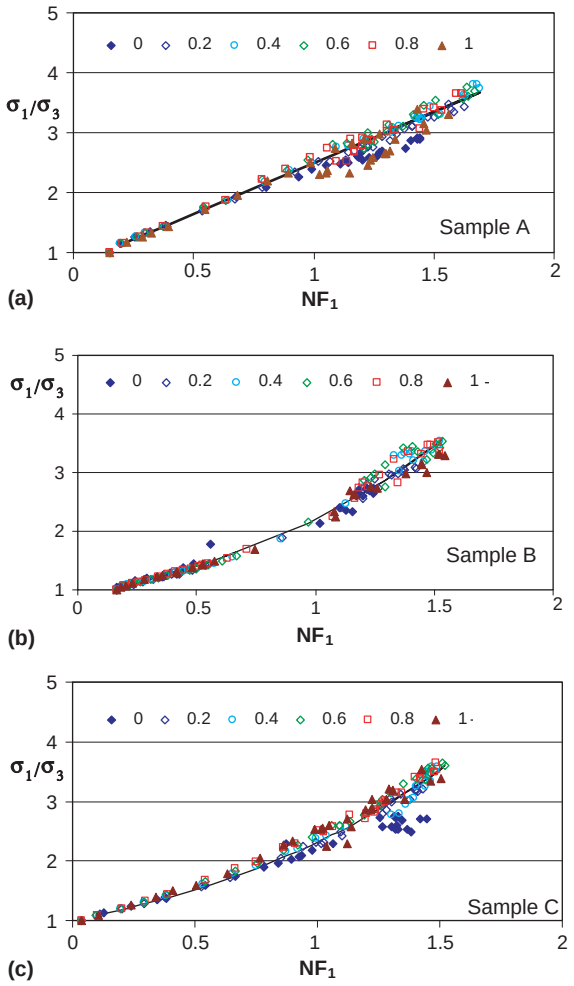

Fig. 13. Principal stress ratio versus NF_1 for Group II.

be insignificant in the present study. The relative difference in shear strength of drained tests along various stress paths is also not affected by anisotropy.

Two failure models predicted the friction angles of the samples. Excellent prediction in friction angle (only 6% relative error) was found for the isotropic sample. The performance of the two models degraded slightly for the anisotropic samples. The worst prediction is only off by 12%. This is good for engineering usage. The model proposed by Ogawa and his coworkers was found to be slightly better. The accuracy is within 5% of the actual value for 90% of the cases.

The study of microscopic information showed that the obliquity relates better with contact normal force (direction + magnitude) than with the unit contact normal (direction only). A linear relationship was found between obliquity and NF_1 for the isotropic sample. An exponential relationship was found for the anisotropic samples. Also, the usefulness of DEM on microscopic analysis is demonstrated in the present study.

Future effort will focus on analyzing other micromechanical information of these drained tests. The result will be very helpful to the development of the linkage between micromechanical information and the

macroscopic parameters such as shear strength, stress–strain behavior, and deformation behavior of granular materials. Finally, a constitutive model based on micromechanics can be developed.

References

Kulhawy, F.H., Mayne, P.W., 1990. Manual on Estimating Soil Properties in Foundation Design. EPRI, Palo Alto, CA.

Lade, P.V., 1977. Elasto-plastic stress–strain theory for cohesionless soil with curved yield surfaces. Int. J. Solids Struct. 13, 1019–1035.

Lade, P.V., 1984. Chapter 20: Failure criterion for frictional materials. In: Desai, C.S., Gallagher, R.H. (Eds.), Mechanics of Engineering Materials. Willey, London, pp. 385–402.

Lin, X., Ng, T.-T., 1997. A three dimensional element model using arrays of ellipsoids. Geotechnique, London 47 (2), 319–329.

Ng, T.-T., 1999. Fabric study of granular materials after compaction. J. Engrg. Mech. ASCE 125 (12), 1390–1394.

Ng, T.-T., 2001. Fabric evolution of ellipsoidal arrays with different particle shapes. J. Engrg. Mech. ASCE 127 (10), 994–999.

Ng, T.-T., 2002. Hydrostatic boundaries in discrete element methods. In: Discrete Element Methods: Numerical Modeling of Discontinua, Geotechnical Special Publication, No. 117, ASCE, pp. 47–51.

Ng, T.-T., 2004. Behavior of ellipsoids of 2 sizes. J. Geotech. Geoenviron. Engrg 130 (10).

Ogawa, S., Mitsui, S., Takemure, O., 1974. Influence of the intermediate principal stress on mechanical properties of a sand. In: Proc. 29th Annual Meeting of JSCE, Part 3, pp. 49–50.

Rothenburg, L., Barthurst, R.J., 1992. Micromechanical features of granular assemblies with planar elliptical particles. Geotechnique 42 (1), 79–95.

Scheidegger, A.E., 1965. On the statistics of the orientation of bedding planes, grain axes and similar sedimentological data. US Geol. Survey 525, 164–167.

Watson, G.S., 1966. The statistics of orientation data. J. Geol. 74, 786–797.

Woodcock, N.H., 1977. Specification of fabric shapes using an eigenvalue method. Geol. Soc. Amer. Bull. 88, 1231–1236.